phra were
agma history

Bogoslof is also one of only two subaerial volcanoes in the Aleutian Islands located significantly behind the main axis of volcanic vents. Amak Island, the other backarc center, has erupted basalts that are more typical of Aleutian arc tholeiites, with plagioclase, pyroxenes, and Fe-Ti oxides, and notable absence of amphibole (Marsh and Leitz 1978). The composition of lavas erupted from these two centers provide the only insight into the subarc mantle in the Aleutians from locations with greater slab depths.

The remote setting and wilderness designation of Bogoslof Island challenged monitoring during the 2016–2017 eruption (Coombs et al. 2018). Tephra samples were only collected on three occasions: when ash fell on the distant communities Nikolski and Dutch Harbor in the Aleutian Islands, and when ash fell on a boat off Cape Kovrizhka (Fig. 1). No proximal samples were collected until a year after the eruption ended. Despite this, remote seismic monitoring from nearby Unmak and Unalaska Islands (Tepp et al. 2019; Searcy and Power 2019), infrasound (Lyons et al. 2019a), lightning (Van Eaton et al. 2019), satellite (Lopez et al. 2019; Schneider et al. 2019), and rare direct observations were pieced together to detect explosive events, providing some insight on the mechanisms of eruption (Wech et al. 2018; Lyons et al. 2019b).

In this paper, we describe the texture, petrology, and geochemistry of the available physical products erupted during the 2016–2017 Bogoslof eruption, including samples of distal tephras from three explosive events and proximal samples collected in August 2018 after the conclusion of the eruption. These proximal samples were only collected from the surface of the island and likely represent the final phase of the eruption. We also report compositions for samples from 1992 and other historical eruptions collected during a visit to the island in 1994 but unpublished until now. The unusual eruption of an amphibole-bearing basalt provides important insight into potentially more ubiquitous but hidden magmatic processes in arcs globally.

posted at https://environment.wsu.edu/facilities/geoanalytical-lab/technical-notes/. Samples 18CW100-10B and 18CW103-4 were analyzed twice to demonstrate analytical reproducibility. An additional ten samples were analyzed, also at Washington State University, from a 1994 field expedition and included eight samples from the 1992 lava dome, one from the 1926 dome, and one from the 1796 dome.

Proximal products of the 2016–2017 Bogoslof eruption can be categorized into three major types: (1) basaltic scoria, (2) light-colored pumice, and (3) dense crystalline lavas exposed in an uplifted area emplaced as early as December 2016 (Fig. 2). The texture and mineralogy of these generalized lithologies are listed below, along with prominent inclusions of mafic and silicic material.

Basaltic scoria and dense blocks were the dominant clast type found on the surface of the island in 2018. They range in size from lapilli to large 2 m bombs and in density from dense to highly vesicular scoria. All are dark in color with 1–2 mm plagioclase and amphibole phenocrysts visible in hand-sam-203.1000061(de)15.10000038(ns)20(i5(y)73.199996960002338(65.6534118

Vesicle-free grains with a dense interlocking network of feldspar microlites, including sanidine, and sometimes alteration minerals including clays and pyrite, comprise 15–40% of the non-crystal fraction (Fig. 3c, d) likely correlating with the uplifted 2016–2017 lithologies (Fig. 2c). The proportion of these grain types decreased from almost 40% of the non-crystalline

Table 1 Representative bulk compositions from Bogoslof 2016–2017 eruption

Sample ID	18CW100-10A	18CW105-1A	18CW100-27	18CW100-13B	18CW105-1B

Bulk compositions of samples collected on Bogoslof range from basalt to trachyte (48–67 wt% SiO_2; Fig. 4). The compositional trend forms a higher alkali series than Aleutian arc-front volcanoes such as nearby Okmok and Makushin, but overlaps compositions at Amak, the other backarc volcanic center to the east (Marsh and Leitz 1978; Fig. 1). Both Bogoslof and arc-front mafic to intermediate compositions are tholeiitic following Miyashiro's (1974) classification.

All 2016–2017 scoriaceous material is basalt to trachybasalt (48–51 wt% SiO_2[1]). These samples overlap with compositions of the 1926 and 1992 lava domes, although 1992 samples have compositions extending to slightly higher SiO_2 (~ 52 wt%, Fig. 4). A larger gabbroic and quenched vesicular mafic inclusion were separated for whole rock analysis and fall in the same general compositional range as the basaltic scoria. The gabbroic inclusion has > 0.5 wt% higher K_2O concentration and > 2× concentrations of Rb, Ba, and Cs than other basalts at the same SiO_2 concentration (Table 1, Figs. 5 and 6). All basalts have enriched REE concentrations, chondrite-normalized La/Yb = 5–6, and lack significant Eu anomalies (Fig. 7). Matrix glass was analyzed in both the quenched mafic inclusion and its host scoria. In both samples, the glass fraction is a more evolved trachyandesite with 60–63 wt% SiO_2 and higher K_2O concentrations than any whole rock compositions from Bogoslof (Fig. 5). Matrix glass in the more microlitic host glass is slightly more evolved (higher SiO_2, lower MgO), but notably has lower K_2O despite the apparent absence of K-bearing minerals in the groundmass.

Rocks exposed in the December 2017 uplifted area south of the main 2016–2017 vent are dense, dome-like tholeiitic trachyandesites (Fig. 4). These intermediate compositions have notably lower alkali (Na_2O, K_2O) and higher CaO concentrations than basaltic matrix glass at similar SiO_2 (Fig. 5). Trace element concentrations of Sr, Ga, and Y are similar to the basalts, Sc, V, Cr, Ni, Cu, Zn, and MREEs are lower than basalts, and Rb, Ba, LREEs, HREEs, and other high-field strength elements (e.g., NbTm[().)]TJ.a0.79999923(sh)s, HREEs96TL92

to 67 wt% SiO_2 (Fig. 5). This compositional range includes analyses of rare microlite-free glass to highly microlitic melt residue (Fig. 3). Compositions trend towards and overlap with the matrix glass measured in the mafic enclave and its host from bulk rock samples (Fig. 5).

Amphibole-, clinopyroxene-, and plagioclase-hosted melt inclusions separated from the uppermost few meters of proximal pyroclastic deposits of the 2016–2017 eruption have glass compositions largely overlapping that of the distal tephra matrix glass (Fig. 8). Some plagioclase and clinopyroxene compositions are more evolved with lower K_2O than basalt matrix glasses, and these inclusions overlap the compositional range of the trachyte pumice. Chlorine concentrations in melt inclusions are actually lower on average than matrix glasses, but still higher than Cl in the evolved trachyte pumice. Sulfur concentrations, not measured in matrix glass, reach up to 3000 ppm, but are lower in the more evolved inclusions with > 60 wt% SiO_2, and are also lower in amphibole-hosted inclusions. Preliminary water concentrations of 1.9 and 2.9 wt%

in two plagioclase-hosted melt inclusions and 2.7, 3.2, and

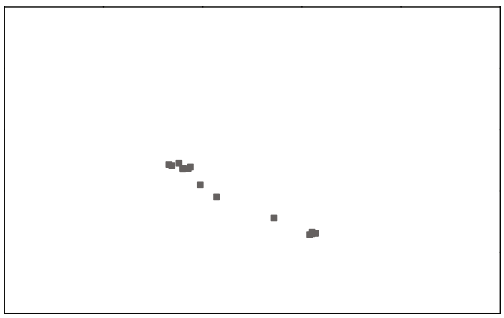

boundary. Composition of the rims is characterized by 13.5–14 wt% MgO and 10–11 wt% FeO(t). The composition of rims is homogenous and the same across phenocrysts, whereas the composition of individual cores is homogenous but variable between different phenocrysts.

Olivine is present exclusively as microlites and rare microphenocrysts with approximately 64 mol.% of forsterite content. Similar to olivine, orthopyroxene also occurs only as microlites. Their composition is bimodal with one mode characterized by approximately En_{53} and the other by En_{66}.

Trachyte pumice

Two populations of plagioclase phenocrysts are present in the trachyte pumice. (1) Oscillatory-zoned phenocrysts with An_{65} to An_{29} compositions, with the compositions gradually changing to more sodic values near the rim. (2) Phenocrysts with euhedral $An_{82–91}$ cores surrounded by oscillatory-zoned $An_{35–58}$ rims (Fig. 9c). Both populations have similar rim compositions but only the core composition of the second type match the 2016–2017 basalt.

Clinopyroxene phenocrysts in light pumice exhibit relatively constant composition. Starting with an En_{37} core with oscillatory variations towards the rim between En_{36} and En_{38} (Fig. 10c). This composition overlaps considerably with clinopyroxene phenocrysts from the trachyandesite. Although amphibole phenocrysts are absent in the pumice, there are abundant opaque pseudomorphs of amphibole (Fig. 11c). Orthopyroxene is present in light pumice as En_{69} microlites.

Biotite occurs in pumices as euhedral to subhedral 0.4–1.0 mm-long tabular phenocrysts, as well as microlites. Their compositions appear to be homogeneous and nearly constant across crystals with 13.8–18.1 wt% FeO(t), 12.7–14.1 wt% MgO, 3.7–4.3 wt% TiO_2, and 0.18–0.35 wt% MnO. Composition of biotite in light pumices is conspicuously different from the composition of accidental biotite grains found in the January 31, 2017 volcanic ash deposits (see online Supplementary Material).

Fe-Ti oxides in pumice include both titanomagnetite and

olivine, which must have crystallized earlier in overall magmatic history driving MgO and Ni to lower concentrations observed in all erupted samples at Bogoslof.

The highly microlitic and diktytaxitic textures in 85–90% of basaltic tephra grains (Fig. 3) are typical of dome or cryptodome eruptive products which are dominated by slow magma ascent and shallow pre-eruptive storage (Gaunt et al. 2016

crystallization seen in basalt matrix glasses (following Barclay and Carmichael 2004 phase relationships, Fig. 13). Elements more strongly influenced by feldspar, such as Sr and Al_2O_3, have a slightly curved evolution supporting such a model.

Davidson et al. (2007) proposed that a zone of amphibole crystallization and accumulation in the mid-crust influences

domes in June and August 2017, were to the north of this uplifted area (Waythomas et al. 2019a).

The trachyandesite composition of rocks collected from the base of the uplifted dome, and as ballistics scattered across the island in August 2018, are a unique composition from the basalts and trachyte pumice and are the only erupted material with sanidine-plagioclase-cristobalite groundmass mineralogy (Fig. 2). Tephra samples sometimes have identical feldspar-cristobalite matrix as fresh proximal samples, but also often also include clay-like mineral compositions of feathery crystalline growths that could be a result of hydrothermal alteration and/or glass devitrification (Fig. 3). No glass has been observed associated with the trachyandesite groundmass

also provide insight into the magmatic source of cryptic amphibole signatures seen in arcs worldwide.

Acknowledgments

Alaska Division of Geological & Geophysical Surveys Raw Data File 2018: 1-29 p. https://doi.org/10.14509/29843

Rutherford MJ, Hill P (1993) Magma ascent rates from amphibole breakdown: an experimental study applied to the 1980–1986 Mount St. Helens eruptions. J Geophys Res 98:19667–19685

Schneider DJ, Van Eaton AR, Wallace KL (2019) Satellite observations of the 2016–17 eruption of Bogoslof volcano: aviation and ash fallout hazard implications from a water-rich eruption. Bull Volcanol (part of the Bogoslof Topical Collection)

Searcy CK, Power JA (2019) Seismic character and progression of explosive activity during the 2016–2017 eruption of Bogoslof volcano, Alaska. Bull Volcanol. https://doi.org/10.1007/s00445-019-1343-4

Sigurdsson H, Shepherd JB (1974) Amphibole-bearing basalts from the submarine volcano Kick'em-Jenny in the Lesser Antilles island arc. Bull Volcanol 38:891. https://doi.org/10.1007/BF02597097

Tepp G, Dziak R, Haney M, Lyons J, Searcy C, Matsumoto H, Haxel J (2019) Seismic and hydroacoustic observations of the 2016–17 Bogoslof Eruption. Bull Volcanol. https://doi.org/10.1007/s00445-019-1344-3

Turner S, Foden J, George R, Evans P, Varne R, Elburg M, Jenner G (2003) Rates and processes of potassic magma evolution beneath Sangeang Api volcano, east Sunda arc, Indonesia. J Petrol 44:491–515. https://doi.org/10.1093/petrology/44.3.491

Van Eaton AR, Schneider DJ, Smith CM, Haney MM, Lyons JJ, Said R, Fee D, Holzworth RH, Mastin LG (2019) Did ice-charging generate volcanic lightning during the 2016–2017 eruption of Bogoslof volcano, Alaska? Bull Volcanol (part of the Bogoslof Topical Collection)

Waters LE, Cottrell E, Kelly K, Coombs ML (2017) Calc-alkaline liquid lines of descent produced under oxidizing conditions: an experimental and petrologic study of basaltic tephras from the Western Aleutians, AK. Abstract V11B-0343 presented at 2017 AGU Fall Meeting, New Orleans, LA, 11-15 Dec.

Waythomas CF, Cameron CE (2018) Historical eruptions and hazards at Bogoslof Volcano, Alaska. U.S. Geol Surv Sci Investig Rep 2018-5085:1–54

Waythomas CF, Angeli K, Wessels RL (2019a) Evolution of the submarine-subaerial edifice of Bogoslof volcano, Alaska, during its 2016–2017 eruption based on analysis of satellite imagery. Bull Volcanol (part of the Bogoslof Topical Collection)

Waythomas CF, Loewen MW, Wallace KL, Cameron CE, Larsen JF (2019b) Geology and eruptive history of Bogoslof volcano. Bull Volcanol (part of the Bogoslof Topical Collection)

Wech A, Tepp G, Lyons J, Haney M (2018) Using earthquakes, T waves, and infrasound to investigate the eruption of Bogoslof Volcano, Alaska. Geophys Res Lett 45:6918–6925. https://doi.org/10.1029/2018GL078457

White J, Houghton B (2000) Surtseyan and related phreatomagmatic eruptions. In: Sigurdsson H, Houghton B, Rymer H, Stix J, McNutt S (eds) , 1st edn. Academic Press, Encyclopedia of volcanoes, pp 495–511

White J, Schipper C, Kano K (2015) Submarine explosive eruptions. In: Sigurdsson H, Houghton B, McNutt S, Rymer H, Stix J (eds) Encyclopedia of volcanoes, 2nd edn. Academic Press, pp 553–569

Yogodzinski GM, Brown ST, Kelemen PB, Vervoort JD, Portnyagin M, Sims KWW, Hoernle K, Jicha BR, Werner R (2015) The role of subducted basalt in the source of island arc magmas: evidence from seafloor lavas of the Western Aleutians. J Petrol 56:441–492. https://doi.org/10.1093/petrology/egv006